

Disorder engineering and conductivity dome in ReS₂ with electrolyte gating

Dmitry Ovchinnikov^{1,2}, Fernando Gargiulo³, Adrien Allain^{1,2}, Diego José Pasquier³, Dumitru Dumcenco^{1,2}, Ching-Hwa Ho⁴, Oleg V. Yazyev³, Andras Kis^{1,2*}

¹*Electrical Engineering Institute, École Polytechnique Fédérale de Lausanne (EPFL), CH-1015 Lausanne, Switzerland*

²*Institute of Materials Science and Engineering, École Polytechnique Fédérale de Lausanne (EPFL), CH-1015 Lausanne, Switzerland*

³*Institute of Physics, École Polytechnique Fédérale de Lausanne (EPFL), CH-1015 Lausanne, Switzerland*

⁴*Graduate Institute of Applied Science and Technology, National Taiwan University of Science and Technology, Taipei 106, Taiwan*

**Correspondence should be addressed to: Andras Kis, andras.kis@epfl.ch*

ABSTRACT

Atomically thin rhenium disulphide (ReS₂) is a member of the transition metal dichalcogenide (TMDC) family of materials characterized by weak interlayer coupling and a distorted 1T structure. Here, we report on the electrical transport study of mono- and multilayer ReS₂ with polymer electrolyte gating. We find that the conductivity of monolayer ReS₂ is completely suppressed at high carrier densities, an unusual feature unique to monolayers, making ReS₂ the first example of such a material. While thicker flakes of ReS₂ also exhibit a conductivity dome and an insulator-metal-insulator sequence, they do not show a complete conductivity suppression at high doping densities. Using dual-gated devices, we can distinguish the gate-induced doping from the electrostatic disorder induced by the polymer electrolyte itself. Theoretical calculations and a transport model indicate that the observed conductivity suppression can be explained by a combination of a narrow conduction band and Anderson localization due to electrolyte-induced disorder.

MAIN TEXT

ReS₂ is a member of the family of recently rediscovered transition metal dichalcogenides (TMDCs). In contrast to the more widely studied MoS₂, which preferentially crystallizes in the 2H phase,¹ ReS₂ has a 1T' distorted crystal structure,²⁻⁴ which results in anisotropic optical, electrical and vibrational properties.⁴⁻⁷ Recent Raman spectroscopy^{3,8} and photoluminescence measurements³ indicate that atomic layers in 1T' ReS₂, unlike those of MoS₂, are decoupled from each other,³ which gives rise to direct band gap preservation from monolayers to bulk crystals. This makes ReS₂ interesting not only in the monolayer, but also in the bulk form for electronic and optoelectronic applications where its optical anisotropy could in principle allow the fabrication of polarization-sensitive photodetectors.^{9,10} Field effect transistors (FET) and integrated circuits made of ReS₂ have already been reported,^{7,11-15} showing anisotropic electrical behavior and mobilities of 1-30 cm²/Vs at room temperature in a limited range of electron doping (below 10¹³ cm⁻²). Here, we use polymer electrolyte gating of mono- and

multilayer ReS₂ to explore a wider range of doping levels in the first ReS₂ electrical double layer transistor (EDLT)¹⁶⁻²³ reported to date. The use of polymer electrolytes can result in charge carrier densities as high as 10¹⁵ cm⁻²,²⁴ largely exceeding doping levels that can be achieved using standard solid gates. Polymer electrolytes are however a known source of disorder. Ions from the polymer electrolyte are in direct contact with the conductive channel²⁵ and act as charged impurities which degrade the mobility of charge carriers.^{25,26} We also include solid bottom gates in our devices, which allow us to modulate the charge density at low temperatures where the polymer electrolyte is frozen and to disentangle the effects of doping and electrolyte-induced disorder.

The aim of this work is to explore the effects of doping and disorder on the electrical conductivity of ReS₂. At high doping levels, a complete and reversible suppression of conductivity in monolayer ReS₂ (Figure 1) is observed. In multilayer flakes the effect is milder and an insulator-metal-insulator sequence is measured instead. Our band structure and transport calculations furthermore shed light on the mechanisms of conductivity suppression.

We first focus on monolayer ReS₂ EDLTs. Device schematic is shown on Figure 1(a) (see Methods and Supplementary Section 1 for the details of device fabrication and EDLT measurements). On Figure 1(b) current I_s as a function of polymer electrolyte voltage (V_{PE}) is presented. Strikingly, the current falls below the instrumentation noise floor at high carrier densities after reaching a maximum. Four-probe measurements reveal that sheet conductivity G reproduces this behavior, thus ruling out the possibility of a contact resistance effect (see Supplementary Figure S1). In the main text we concentrate on devices measured using PS-PMMA-PS:[EMIM]-[TFSI] as the electrolyte. Experiments using LiClO₄-based polymer electrolyte gave essentially the same result (Supplementary Figure S2). Although a strong hysteresis is present in our measurements, the initial conductivity is restored at the end of the voltage sweep, indicating that no degradation has occurred in our device. Furthermore, we swept V_{PE} 10 times in a different device (Supplementary Figure S3), and found good current stability. The distinct behavior of the conductivity with suppression at high carrier densities was observed in all monolayer ReS₂ devices studied (six monolayer ReS₂ EDLTs).

Since the observed effect is not related to contact resistance, electrolyte type or cycling history, we consider electrolyte-induced disorder as the possible origin of the observed conductivity suppression at high doping levels. To reveal the possible influence of polymer electrolyte on the conductivity, we perform consecutive measurements on the same device before and after deposition of the electrolyte, as a function of temperature. In addition to the polymer electrolyte, we use a back-gate stack containing a high- κ dielectric to modulate the charge density in our Hall bar devices (Inset of Figure 2c and Supplementary Section 1).

The back-gate voltage V_{bg} dependence of the sheet conductivity G for different temperatures is shown on Figure 2(a). On the left panel, the conductivity prior to the electrolyte deposition is shown. In the subsequent panels, G as a function of V_{bg} is recorded after freezing the electrolyte at a given V_{PE} (freezing point ~180-230 K, Supplementary Section 1). Without the electrolyte, we observe a metal-insulator transition around $V_{bg} = 5.6$ V and field-effect mobilities of $\mu_{FE} \sim 3$ cm²/Vs, consistent with other studies of ReS₂.^{7,11,14,15} As soon as the electrolyte is deposited and $V_{PE} = 0$ V is applied (second panel), the overall conductivity decreases and the sample displays a purely insulating behavior. Increasing the V_{PE} further results in a gradual decrease of conductivity (Figure 2(a), from left to right). To quantify the changes in insulating behavior, we tracked the conductivity dome as a distinct feature in our experiments. We fit our data in this insulating state with the thermally-activated transport model $G(T) = G_0 e^{-E_a/k_B T}$, where G_0 is a constant conductivity, E_a is the activation energy, k_B the Boltzmann constant and T the temperature. For all values of V_{PE} we could achieve a good fit in the range between 70 K and 150 K (Figure 2(b)). Figure 2(c) shows E_a as a function of

V_{PE} for $\Delta V_{\text{bg}} = 0 \text{ V}$, where $\Delta V_{\text{bg}} = V_{\text{bg}} - V_{\text{bg}}^{\text{max}}$. We can see that increasing the electrolyte voltage results in a significant increase of the activation energy (Figure 2(c)). This is in contrast to band-like transport and metallic state emerging at high carrier densities in the case of solid-gated devices before electrolyte deposition. The same behavior was observed in devices fabricated on thicker SiO_2 substrates (see Supplementary Figure S4).

Further evidence of a major role of disorder comes from our analysis of the thickness dependence. We performed similar measurements on ReS_2 with thicknesses ranging from 0.75 nm (monolayer) to 21 nm. Figure 3(a) presents the room-temperature field-effect curves of ReS_2 EDLTs with different thickness. For clarity, only sweeps in the reverse direction, from $V_{\text{PE}} = 2.5 \text{ V}$ to $V_{\text{PE}} = -0.5 \text{ V}$, are shown. There is a stark contrast between the case of monolayer and thicker layers. First, monolayer EDLTs are the only devices that switch off at high doping levels, while the multilayers, although displaying a conductivity dome, remain largely conductive at $V_{\text{PE}} = 2.5 \text{ V}$. Second, multilayer devices are systematically 4-8 times more conductive than monolayers in the ON state. Among multilayers ($>2\text{L}$), device-to-device variation in doping and hysteresis are of the same order of magnitude, making these curves essentially undistinguishable. Although it is expected that monolayers are more sensitive to surface disorder, such a drastic difference was not observed between monolayer and multilayer MoS_2 , WSe_2 or MoSe_2 (see Supplementary Section 6).

We have performed measurements at different temperatures using a 10 nm thick flake as a representative of multilayer ReS_2 (see also Supplementary Figure S6). On Figure 3(b) we summarize our measurements on this device. Moving from the conduction band edge, the device shows weakly insulating behavior. Around $V_{\text{PE}} = 0.5 \text{ V}$, transition to the metallic regime occurs, which is consistent with recent measurements on multilayer ReS_2 with a solid gate.¹² After the conductivity dome, the device undergoes a transition back to the insulating state at $V_{\text{PE}} = 2.3 \text{ V}$. We further examine this second transition. We have performed Hall effect measurements in another multilayer (three layers, 2.2 nm thickness), where we have measured simultaneously Hall mobility μ_{Hall} and carrier density $n_{2\text{D}}$ (Supplementary Section 8). Carrier densities of up to $2.3 \times 10^{13} \text{ cm}^{-2}$ could be induced at high positive V_{PE} . We have performed three cooldowns: for charge densities left of the conductivity dome ($V_{\text{PE}} = 0.9 \text{ V}$), near the conductivity maximum ($V_{\text{PE}} = 1.6 \text{ V}$) and right above it ($V_{\text{PE}} = 2.1 \text{ V}$). Cooldowns were performed at close values of V_{PE} and we could continuously modulate the carrier density between neighboring cooldowns by applying V_{bg} to the silicon substrate covered by 270 nm SiO_2 , (Supplementary Figure S8b). This allowed us to measure the Hall mobility for each specific value of V_{PE} and $n_{2\text{D}}$. The striking feature of our measurements is the significant decrease of mobility at the same values of carrier density for increasing values of V_{PE} , as shown on Figure 3(c). During the first cooldown ($V_{\text{PE}} = 0.9 \text{ V}$), we measured metallic behavior with Hall mobility values exceeding $200 \text{ cm}^2/\text{Vs}$ at low temperatures (red filled markers). With V_{PE} increasing to 1.6 V, the mobility at the same carrier density decreases by the factor of 8 (red empty markers). The same behavior is observed while moving from second to third cooldown. Finally, the material becomes insulating as both the V_{PE} and $n_{2\text{D}}$ are increased (see also Figure S8).

The insulating state at high carrier densities is a distinct feature of multilayer ReS_2 EDLTs, in contrast to other semiconducting TMDCs,^{16,18,27} which exhibit band-like transport (see discussion in Supplementary Section 6). On Figure 4(a), we show the dependence of the reduced activation energy $w = -d(\ln R) / d(\ln T)$ ²⁸ on the temperature for the 10 nm thick flake previously discussed on Figure 3(b). We distinguish two types of behavior. In the 96–172 K temperature range, the temperature dependence of the resistance can be fitted using Mott variable range hopping (VRH)²⁹ behavior $R \propto \exp\left[\left(T_0 / T\right)^{1/3}\right]$. The coefficient extracted from

the $w - \ln T$ dependence is 0.36 (red line on Figure 4(a)), which fits well to the VRH model. We find a density of states $D_{2D}^{theory} = 4.17 \times 10^{14} eV^{-1} cm^{-2}$ and localization length $\xi_{loc} \approx 0.35 \div 0.63 nm$ (see also Supplementary Section 11 for effective mass calculations). At lower temperatures, w reaches saturation as a function of $\ln T$, which is an indication of multiphonon hopping regime. We discuss both conduction mechanisms further in Supplementary Sections 9 and 10.

Activation and hopping regimes, observed in ReS₂ at high carrier densities suggest that disorder plays an important role in the observed behavior. Aside from it, there are other possible explanation which should be considered: i) phase transition due to doping, ii) complete filling of the disentangled conduction band (see further text for discussion of the ReS₂ band structure) and iii) influence of the perpendicular electric field on the band structure. These are discussed and ruled out in Supplementary Section 12.

We have performed DFT calculations of the band structure of mono- and multilayer ReS₂ to shed more light on the observed behavior of electrical conductance. Figure 5(a-c) shows the crystal structure of monolayer ReS₂ along with the calculated band structure along high symmetry directions and the integrated density of states (DOS). We find an unusual feature in the band structure – a narrow conduction band almost separated from other bands by a minimum in the DOS, as shown in Figure 5(c), right panel. This feature is present in both mono- (Figure 5(c)) and multilayer ReS₂ (Supplementary Figure S9).

Further on, we concentrate on the quantitative interpretation of our findings. Depending on the effective strength of the interaction between ions and electrons (holes), and the effective mass of the charge carriers, the latter may form a bound state preventing transport. Monolayer ReS₂ has a narrow conduction band ≈ 0.4 eV wide and a large effective mass $m^* = 0.5 m_e$, where m_e is the free-electron mass (for effective masses and bulk ReS₂ band structure see Supplementary Section 11). This makes ReS₂ similar to organic semiconductors such as p-doped rubrene (HOMO bandwidth $D \approx 0.4$ eV, hole effective mass $m_h^* = 0.6 m_e$ ³⁰) that shows a decrease of conductivity and high charge densities^{26,31–33}, albeit without a full conductivity suppression at high charge densities like in the case of monolayer ReS₂.

A fully quantum argument based on Anderson localization sheds light on this reasoning. The ionic positions at the electric double layer are to a large extent random, thus introducing a Coulomb potential that does not reproduce the periodicity of the semiconductor lattice. Assuming that one-electron states of the conduction band of ReS₂ can be described by the tight-binding model, the electrolyte-induced disorder consists of a random but spatially correlated distribution of on-site energies characterized by a finite width W . Classical Anderson localization theory predicts that disorder causes full localization of the one-particle states of two-dimensional lattices, irrespective of the disorder strength W ^{34,35}. Nevertheless, a larger amount of disorder W is generally associated with a shorter localization length ξ ^{36,37}. Electronic transport in the presence of a localized spectrum takes place *via* hopping between localized states with temperature dependence characteristic of an insulator. However, as Anderson localization is ultimately a consequence of destructive interference of the wavefunctions, phase breaking mechanisms (e.g. electron-phonon scattering) that take place over a phase conservation length $L_\phi \leq \xi$ prevent the physical realization of Anderson localization.

An increase of the number of ions at the electrolyte-semiconductor interface translates into the broadening of the overall on-site energy distribution, so that the effective amount of disorder W increases. Therefore, ξ is a decreasing function of V_{PE} . If one assumes that, at fixed temperature, L_ϕ does not vary considerably upon doping, the condition for the onset of the metal-insulator transition is $\xi(V_{PE}^*) \approx L_\phi$. For increasing gate voltage ($V_{PE} > V_{PE}^*$), charge-carrier mobility $\mu(V_{PE})$ is expected to drop faster than inverse linear law, leading to a rapid

decay of conductivity $\sigma \propto n\mu$. We stress that the narrowness of the conduction band is crucial to revealing the wavefunction localization, as the key quantity in Anderson localization is the adimensional disorder strength W/D ^{36,38}. In our opinion, this phenomenon is responsible for such a peculiar behavior of monolayer ReS₂ among other 2D TMDCs.

In order to investigate qualitatively the discussed phenomenon, we consider the following model of electronic transport. We describe the lowest conduction band of ReS₂, highlighted in Figure 5(c), *via* a tight-binding model on a rectangular lattice, with x and y directions corresponding to the parallel and perpendicular directions relative to the "easy" axis (along Re chains). Monovalent point charges (e.g. Li⁺) are placed at a distance $\Delta z = 20$ Å from the plane of the rectangular lattice. In order to guarantee the total charge neutrality of the ionic gate-semiconductor interface, the ionic concentration n_{ions} must be equal to electron concentration $n_{2\text{D}}$. The electrical conductivity has been calculated by means of the Kubo formula^{39,40} assuming linear response to the applied electric field.

The calculated density of states (DOS) shown in Figure 5(d) is characterized by long tails upon increasing n_{ions} . These tails indicate the presence of localized states induced by electrostatic disorder. Moreover, n_{ions} determines the chemical potential μ of the electrons, which shifts further into the conduction band upon the increase of doping. The transport behavior as a function of n_{ions} is ultimately determined by the interplay between the increasingly localized states of the spectrum and the position of the chemical potential within the conduction band. The conductivity σ calculated along x and y directions is shown in Fig. 5(e). Here, a pronounced dome in the conductivity followed by a full suppression of at high carrier densities is observed. The ionic concentration, i.e. the carrier density associated with the peak of the dome, is $n_{\text{ions}}^* = 0.06 \div 0.08$ ions per unit cell. We observe a very good agreement with measured carrier densities extracted from the Hall effect data (Supplementary Figure 8(a)). The anisotropy calculated in the region of the dome, $\sigma_y/\sigma_x = 0.6$ also agrees well with our experimental data. Above certain ionic concentrations the curves along the two directions merge and become undistinguishable. This isotropic regime at high carrier densities could be clearly seen in the experimentally measured two-probe conductivity curves (Supplementary Figure 10). We ascribe this feature to the onset of full localization in the states in the energy region around the chemical potential, *i.e.* those states responsible for transport. Therefore, localization eliminates any preferential direction for transport.

Theoretical intuition suggests how the behavior of conductivity must change in multilayer ReS₂. First, classical scaling theory of Anderson localization in $d = 2 + \varepsilon$ ($\varepsilon > 0$) dimensions predicts that extended states do not disappear entirely, but in the energy spectrum they are separated from localized states by so-called mobility edges. Second, the injection of electrons itself into the conduction band of ReS₂ results in a rapid screening of the Coulomb potential in the bulk of the sample, which is less affected by electrostatic disorder, thus preserving the charge-carrier mobility. These arguments point toward a scenario where the multilayer ReS₂ conductivity is less influenced by disorder than in the case of the monolayer.

In conclusion, we have realized the first transport study of ReS₂ EDLT with thicknesses ranging from one (0.75 nm) to ~ 30 layers (21 nm). We demonstrate that ionic disorder leads to an unusual OFF state at high carrier densities in the case of monolayers. In the case of multilayers, an insulator-metal-insulator sequence as well as a quenching of Hall mobility with increasing V_{PE} were observed. Highly doped state of multilayer ReS₂ is characterized by a hopping mechanisms with small localization length. Due to the unique band structure with a narrow low-energy conduction band ReS₂ stands apart from other TMDCs, where such modulation of conductivity at high carrier densities was not observed. Our transport model quantitatively explains our findings.

ACKNOWLEDGEMENTS

Authors gratefully acknowledge the help and supervision of Prof. Y.-S. Huang with crystal growth. Authors thank O. Lopez Sanchez, Y.-C. Kung, K. Marinov, S. Misra and M. Audiffred for help and motivating discussions. We acknowledge help of D. Alexander, S. Lopatin and S. Lazar for training and support with electron microscopy which was performed using an FEI Titan Themis Cs-corrected TEM at the EPFL Interdisciplinary Centre for Electron Microscopy (CIME). Device fabrication was carried out in the EPFL Center for Micro/Nanotechnology (CMi). We thank Z. Benes (CMi) for technical support with e-beam lithography.

This work was financially supported by funding from the European Union's Seventh Framework Programme FP7/2007-2013 under Grant Agreement No. 318804 (SNM) and Swiss SNF Sinergia Grant no. 147607. The work was carried out in frames of the Marie Curie ITN network "MoWSeS" (grant no. 317451). We acknowledge funding by the EC under the Graphene Flagship (grant agreement no. 604391).

MATERIALS AND METHODS

Device fabrication. Flakes of mono- and multilayer ReS₂ were obtained from bulk crystals which were cleaved using an adhesive tape and transferred on a degenerately doped n⁺⁺ Si covered with 270 nm SiO₂. Contacts were fabricated by standard e-beam lithography, followed by evaporation of Pd/Au contacts and liftoff in acetone. Selected devices were also patterned with a second e-beam step and subsequently etched in O₂/SF₆ plasma. Another series of devices was fabricated transferring monolayer flakes on top of local back gates (Cr/Au) covered with 30 nm HfO₂ deposited using atomic layer deposition (ALD).

Supplementary Information: crystal growth, ion gel preparation, electrical and cryogenic measurement, STEM imaging and computational details.

REFERENCES

1. Wang, Q. H., Kalantar-Zadeh, K., Kis, A., Coleman, J. N. & Strano, M. S. Electronics and optoelectronics of two-dimensional transition metal dichalcogenides. *Nat. Nanotechnol.* **7**, 699–712 (2012).
2. Kelty, S. P., Ruppert, A. F., Chianelli, R. R., Ren, J. & Whangbo, M.-H. Scanning Probe Microscopy Study of Layered Dichalcogenide ReS₂. *J. Am. Chem. Soc.* **116**, 7857–7863 (1994).
3. Tongay, S. *et al.* Monolayer behaviour in bulk ReS₂ due to electronic and vibrational decoupling. *Nat Commun* **5**, (2014).
4. Chenet, D. A. *et al.* In-Plane Anisotropy in Mono- and Few-Layer ReS₂ Probed by Raman Spectroscopy and Scanning Transmission Electron Microscopy. *Nano Lett.* (2015).
5. Ho, C. H., Huang, Y. S. & Tiong, K. K. In-plane anisotropy of the optical and electrical properties of ReS₂ and ReSe₂ layered crystals. *J. Alloys Compd.* **317–318**, 222–226 (2001).
6. Cui, Q. *et al.* Transient Absorption Measurements on Anisotropic Monolayer ReS₂. *Small* **11**, 5565–5571 (2015).
7. Liu, E. *et al.* Integrated digital inverters based on two-dimensional anisotropic ReS₂ field-effect transistors. *Nat Commun* **6**, (2015).
8. Feng, Y. *et al.* Raman vibrational spectra of bulk to monolayer ReS₂ with lower symmetry. *Phys. Rev. B* **92**, 54110 (2015).

9. Friemelt, K., Lux-Steiner, M. -Ch. & Bucher, E. Optical properties of the layered transition-metal-dichalcogenide ReS₂: Anisotropy in the van der Waals plane. *J. Appl. Phys.* **74**, 5266–5268 (1993).
10. Ho, C. H., Yen, P. C., Huang, Y. S. & Tiong, K. K. Photoreflectance study of the excitonic transitions of rhenium disulphide layer compounds. *Phys. Rev. B* **66**, 245207 (2002).
11. Corbet, C. M. *et al.* Field Effect Transistors with Current Saturation and Voltage Gain in Ultrathin ReS₂. *ACS Nano* (2014).
12. Pradhan, N. R. *et al.* Metal to insulator quantum-phase transition in few-layered ReS₂. *Nano Lett.* **15**, 8377–8384 (2015).
13. Leicht, G., Berger, H. & Levy, F. The growth of n- and p-type ReS₂ and ReSe₂ single crystals and their electrical properties. *Solid State Commun.* **61**, 531–534 (1987).
14. Lin, Y.-C. *et al.* Single-Layer ReS₂: Two-Dimensional Semiconductor with Tunable In-Plane Anisotropy. *ACS Nano* (2015).
15. He, X. *et al.* Chemical Vapor Deposition of High-Quality and Atomically Layered ReS₂. *Small* **11**, 5423–5429 (2015).
16. Ye, J. T. *et al.* Superconducting Dome in a Gate-Tuned Band Insulator. *Science* **338**, 1193–1196 (2012).
17. Jo, S., Costanzo, D., Berger, H. & Morpurgo, A. F. Electrostatically Induced Superconductivity at the Surface of WS₂. *Nano Lett.* **15**, 1197–1202 (2015).
18. Shi, W. *et al.* Superconductivity Series in Transition Metal Dichalcogenides by Ionic Gating. *Sci Rep* **5**, (2015).
19. Saito, Y. *et al.* Superconductivity protected by spin-valley locking in ion-gated MoS₂. *Nat. Phys.* **12**, 144–149 (2016).
20. Costanzo, D., Jo, S., Berger, H. & Morpurgo, A. F. Gate-induced superconductivity in atomically thin MoS₂ crystals. *Nat. Nanotechnol.* **11**, 339–344 (2016).
21. Fujimoto, T. & Awaga, K. Electric-double-layer field-effect transistors with ionic liquids. *Phys. Chem. Chem. Phys.* **15**, 8983–9006 (2013).
22. Cho, J. H. *et al.* Printable ion-gel gate dielectrics for low-voltage polymer thin-film transistors on plastic. *Nat. Mater.* **7**, 900–906 (2008).
23. Cho, J. H. *et al.* High-Capacitance Ion Gel Gate Dielectrics with Faster Polarization Response Times for Organic Thin Film Transistors. *Adv. Mater.* **20**, 686–690 (2008).
24. Yuan, H. *et al.* High-Density Carrier Accumulation in ZnO Field-Effect Transistors Gated by Electric Double Layers of Ionic Liquids. *Adv. Funct. Mater.* **19**, 1046–1053 (2009).
25. Gallagher, P. *et al.* A high-mobility electronic system at an electrolyte-gated oxide surface. *Nat Commun* **6**, (2015).
26. Xia, Y., Xie, W., Ruden, P. P. & Frisbie, C. D. Carrier Localization on Surfaces of Organic Semiconductors Gated with Electrolytes. *Phys. Rev. Lett.* **105**, 36802 (2010).
27. Yuan, H. *et al.* Zeeman-type spin splitting controlled by an electric field. *Nat Phys* **9**, 563–569 (2013).
28. Zabrodskii, A. G. The Coulomb gap: The view of an experimenter. *Philos. Mag. Part B* **81**, 1131–1151 (2001).
29. Mott, N. F. Conduction in non-crystalline materials. *Philos. Mag.* **19**, 835–852 (1969).
30. Machida, S. *et al.* Highest-Occupied-Molecular-Orbital Band Dispersion of Rubrene Single Crystals as Observed by Angle-Resolved Ultraviolet Photoelectron Spectroscopy. *Phys. Rev. Lett.* **104**, 156401 (2010).
31. Xie, W., Liu, F., Shi, S., Ruden, P. P. & Frisbie, C. D. Charge Density Dependent Two-Channel Conduction in Organic Electric Double Layer Transistors (EDLTs). *Adv. Mater.* **26**, 2527–2532 (2014).

32. Xie, W., Wang, S., Zhang, X., Leighton, C. & Frisbie, C. D. High Conductance 2D Transport around the Hall Mobility Peak in Electrolyte-Gated Rubrene Crystals. *Phys. Rev. Lett.* **113**, 246602 (2014).
33. Xie, W. & Frisbie, C. D. Organic Electrical Double Layer Transistors Based on Rubrene Single Crystals: Examining Transport at High Surface Charge Densities above 10^{13} cm⁻². *J. Phys. Chem. C* **115**, 14360–14368 (2011).
34. Abrahams, E., Anderson, P. W., Licciardello, D. C. & Ramakrishnan, T. V. Scaling Theory of Localization: Absence of Quantum Diffusion in Two Dimensions. *Phys. Rev. Lett.* **42**, 673–676 (1979).
35. Anderson, P. W. Absence of Diffusion in Certain Random Lattices. *Phys. Rev.* **109**, 1492–1505 (1958).
36. Gargiulo, F. *et al.* Electronic Transport in Graphene with Aggregated Hydrogen Adatoms. *Phys. Rev. Lett.* **113**, 246601 (2014).
37. Economou, E. N. *Green's Functions in Quantum Physics*. **7**, (Springer Berlin Heidelberg, 2006).
38. Evers, F. & Mirlin, A. D. Anderson transitions. *Rev. Mod. Phys.* **80**, 1355–1417 (2008).
39. Kubo, R. Statistical-Mechanical Theory of Irreversible Processes. I. General Theory and Simple Applications to Magnetic and Conduction Problems. *J. Phys. Soc. Jpn.* **12**, 570–586 (1957).
40. Gargiulo, F., Perroni, C. A., Ramaglia, V. M. & Cataudella, V. Electronic transport within a quasi-two-dimensional model for rubrene single-crystal field effect transistors. *Phys. Rev. B* **84**, 245204 (2011).

FIGURES

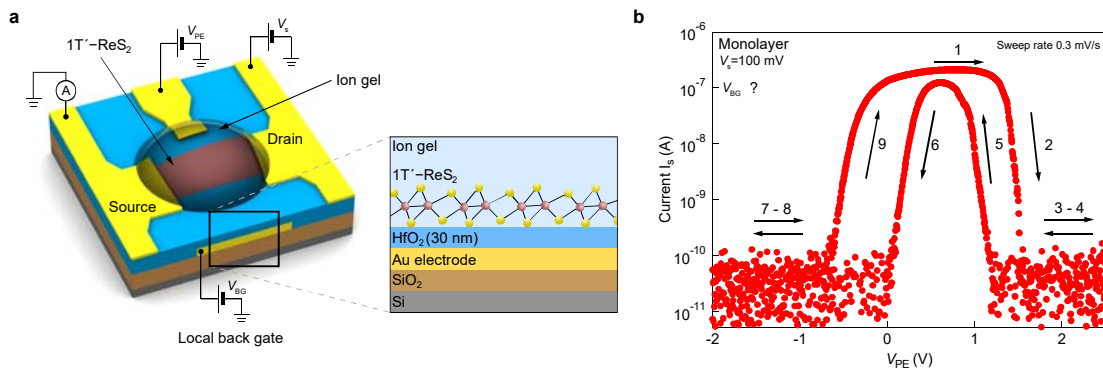


Figure 1. Monolayer ReS₂ room temperature characterization. (a) Schematic of the EDLT based on monolayer ReS₂. (b) Current I_s as a function of polymer electrolyte voltage V_{PE} . Arrows are showing the voltage sweep direction.

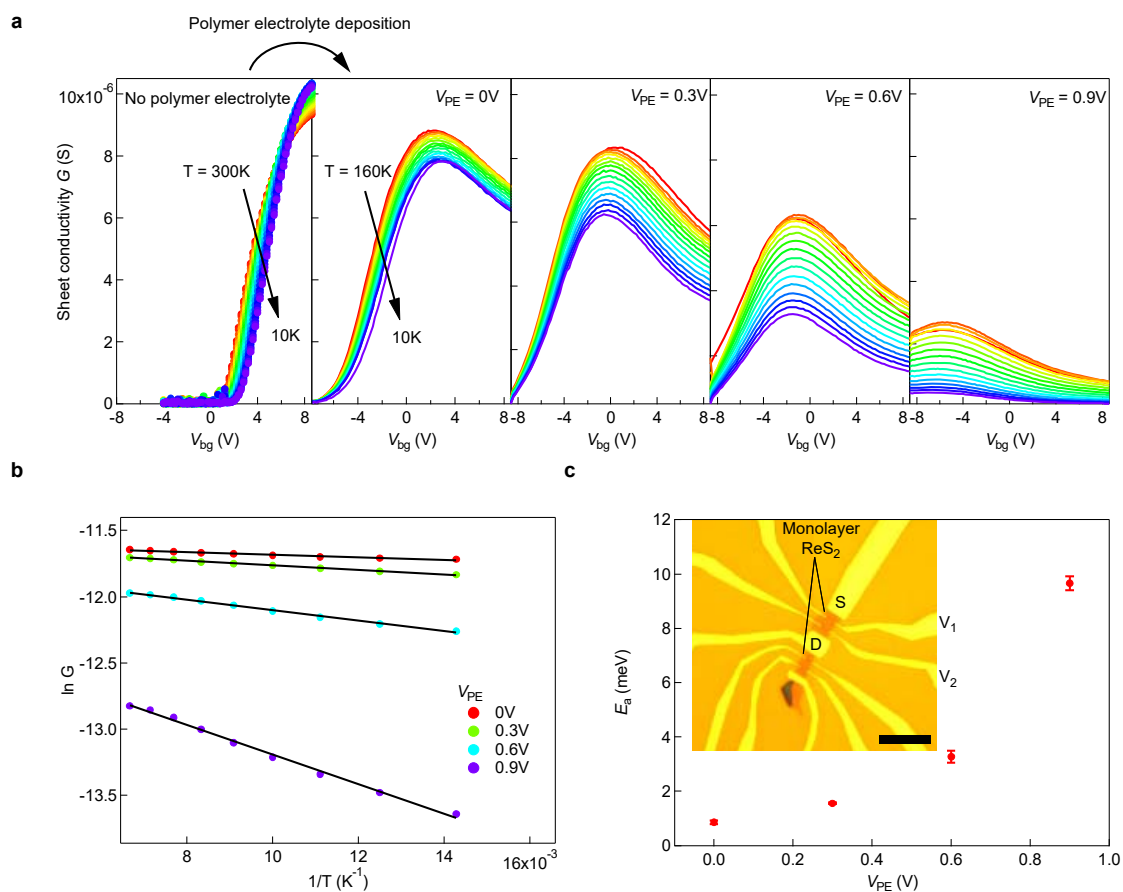


Figure 2. Monolayer ReS₂ with and without the polymer electrolyte. (a) Sheet conductivity G as a function of back-gate voltage V_{bg} prior to PE deposition (left panel) and after PE deposition with different V_{PE} applied. (b) Arrhenius plots for E_a extracted on top of conductivity dome. (c) Activation energy E_a , extracted from the top of the conductivity dome as a function of V_{PE} . Inset - optical image of the device, scale bar - 10 μm .

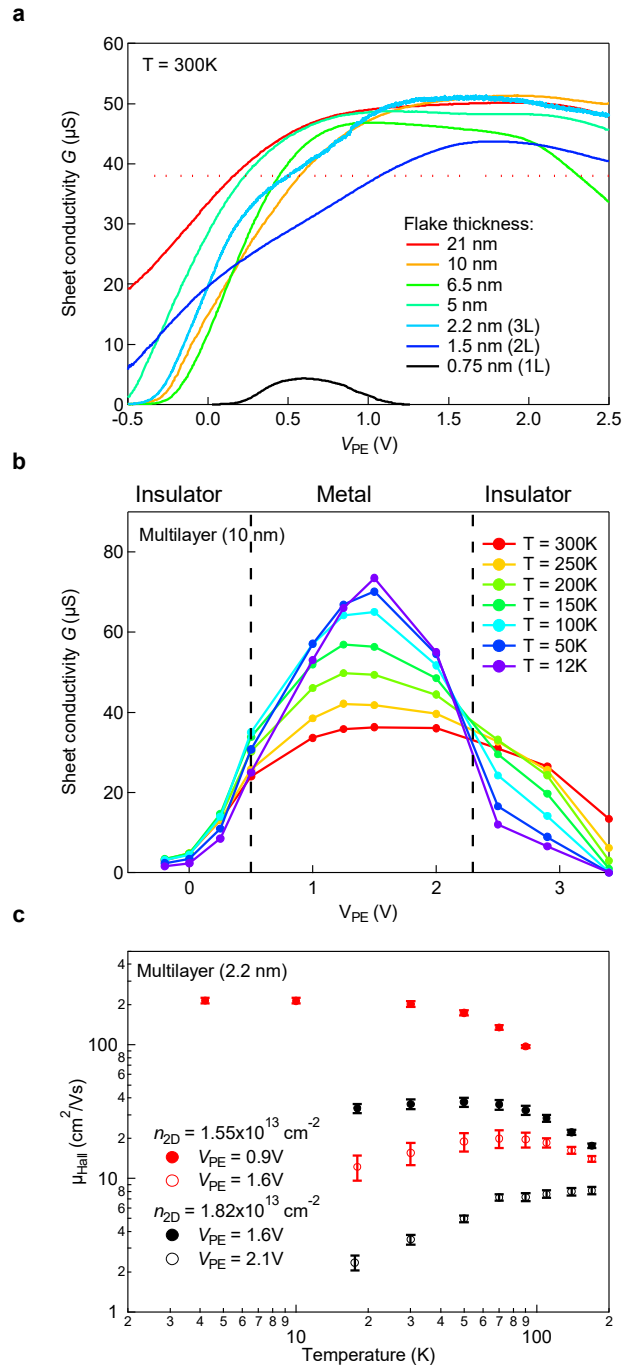


Figure 3. Multilayer ReS₂ - insulator-metal-insulator sequence. (a) Sheet conductivity G as a function of V_{PE} for ReS₂ flakes of different thicknesses. (b) Insulator-metal-insulator sequence for multilayer (10 nm) ReS₂ flake. (c) Hall mobility for the "easy" axis of trilayer ReS₂ (2.2 nm thick) as a function of temperature T for different carrier densities and V_{PE} .

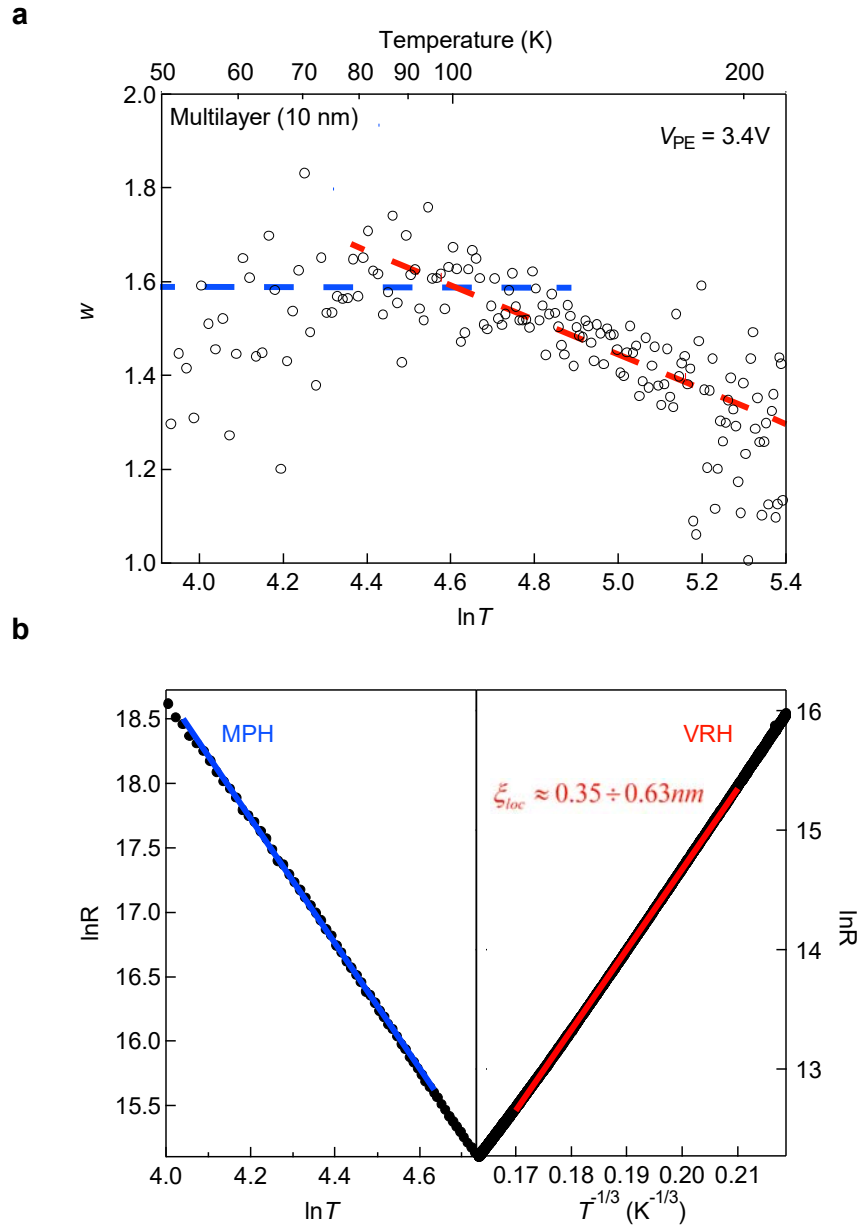


Figure 4. Multilayer ReS₂ - insulating state at high carrier densities. (a) Reduced activation energy w as a function of $\ln T$. Red and blue dashed lines correspond to variable range hopping (VRH) and multiphonon hopping (MPH) regimes respectively. (b) Fits for MPH (left) and VRH (right) in the corresponding range of temperatures.

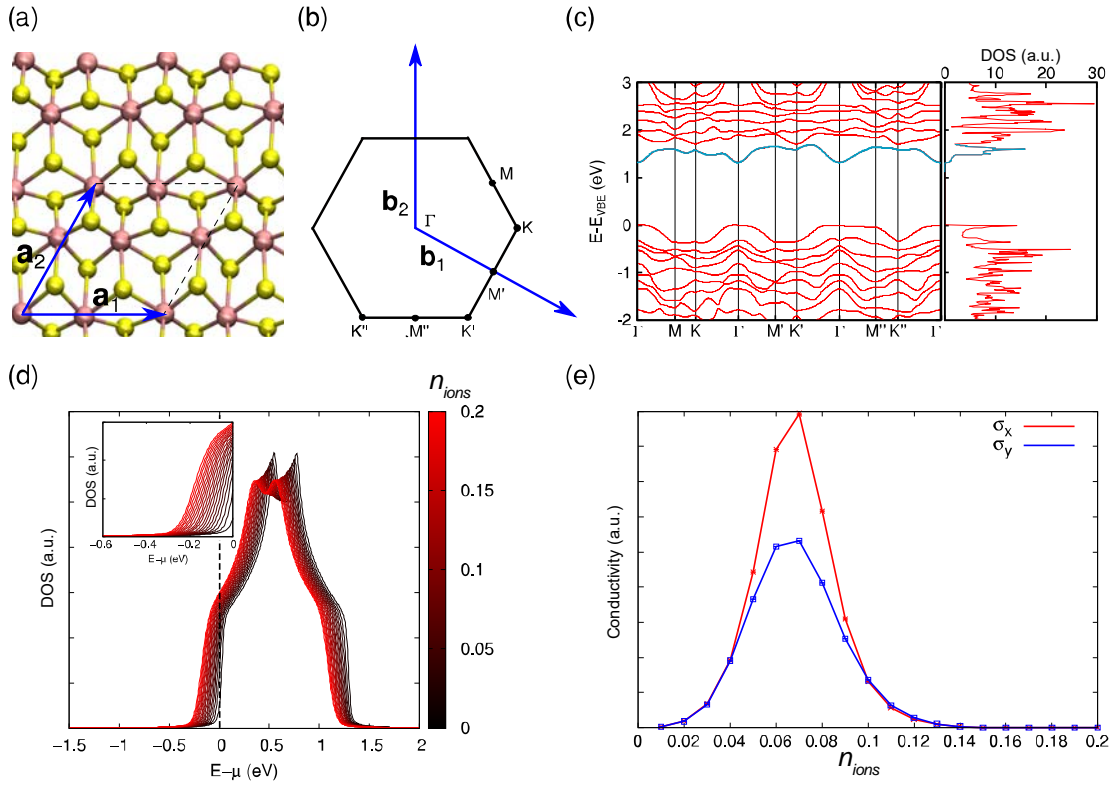


Figure 5. Electronic structure of monolayer ReS_2 from *ab initio* calculations. (a) Ball-and-stick representation of the atomic structure of monolayer ReS_2 . Lattice vectors \mathbf{a}_1 and \mathbf{a}_2 and unit cell (dashed lines) are illustrated. (b) Brillouin zone and primitive vectors \mathbf{b}_1 and \mathbf{b}_2 of reciprocal lattice. (c) Energy bands calculated along high-symmetry directions connecting the vertices defined in (b) and k-integrated density of states (right panel). The lowest energy conductance band as well as its contribution in the DOS are highlighted in purple. (d) Density of states modification due to addition of ions with the concentration $n_{\text{ions}} = (N_+ - N_-)/N_{\text{cells}}$ on top of conductivity channel calculated using our transport model. Color code corresponds to the amount of ions n_{ions} . (e) Conductivities σ_x and σ_y as a function of ionic concentration n_{ions} for directions parallel and perpendicular to the "easy" axis (along Re chains), respectively, calculated using the Kubo formula.